Atmospheric Environment 276 (2022) 119036

Contents lists available at ScienceDirect

Atmospheric Environment

journal homepage: www.elsevier.com/locate/atmosenv

Using nitrogen and oxygen stable isotopes to analyze the major NO_x sources to nitrate of $PM_{2.5}$ in Lanzhou, northwest China, in winter-spring periods

Meiju Yin [a,b], Hui Guan [a,*], Li Luo [c], Huayun Xiao [a], Zhongyi Zhang [d]

[a] State Key Laboratory of Environmental Geochemistry, Institute of Geochemistry, Chinese Academy of Sciences, Guiyang, 550081, China
[b] University of Chinese Academy of Sciences, Beijing, 100049, China
[c] State Key Laboratory of Marine Resource Utilization in South China Sea, Hainan University, Haikou, 570228, China
[d] Key Laboratory of the Causes and Control of Atmospheric Pollution, East China University of Technology, Nanchang, 330000, China

HIGHLIGHTS

- $PM_{2.5}$, water-soluble inorganic ions, $\delta^{15}N–NO_3^-$ and $\delta^{18}O–NO_3^-$ were characterized in Lanzhou.
- The contribution of coal combustion to atmospheric gradually increased in winter.
- In spring, the aerosol components of mineral dust have a catalytic effect on the heterogeneous reactions of N_2O_5.

GRAPHICAL ABSTRACT

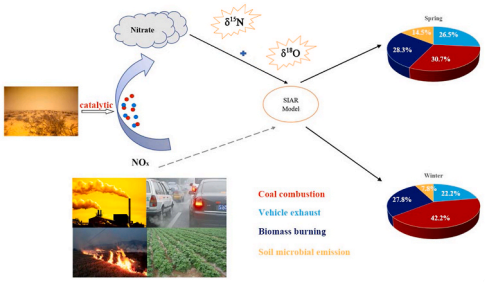

ARTICLE INFO

Keywords:
Air pollution
Source apportionment
Winter-spring $PM_{2.5}$
Nitrate aerosol
Stable isotope

ABSTRACT

Nitrate (NO_3^-) is a standout amongst the essential inorganic aerosols in the atmosphere. Stable isotopic constraint is a robust means to identify the oxidation mechanisms for atmospheric particulate nitrate (NO_3^-) production. However, rarely studies noted the heavily polluted environments of northwest China. In this study, fine particulate matter ($PM_{2.5}$) samples were gathered starting from December 2017 till April 2018 in the urban zone of Lanzhou, northwest China, and water-soluble ions, $\delta^{15}N–NO_3^-$ and $\delta^{18}O–NO_3^-$, were analysed to explore the possible sources of NO_3^- aerosols. The average concentration of $PM_{2.5}$ was 63.1 ± 22.6 μg m^{-3}, indicating severe fine PM pollution. The formation of secondary pollutants NO_3^-, SO_4^{2-}, and NH_4^+ concentrations were higher in winter than in spring. The Ca^{2+}, Na^+, and Mg^{2+} concentrations were much higher in spring than in winter, and the concentration of Ca^{2+} was higher than those in other cities, which implies that the $PM_{2.5}$ concentration is significantly affected by dust. The $\delta^{15}N$ and $\delta^{18}O$ values were lower in warmer months, confirming that the contribution of each nitrate source and the oxidation pathways change similarly as the season transforms from cold to warm. The nitrogen sources were analysed using stable isotope analysis in R (SIAR). The results showed that coal combustion, biomass burning, vehicle exhausts, and soil microbial emissions account for 42.2 ± 9.9%, 27.8 ± 16.2%, 22.2 ± 12.3%, and 7.7 ± 5.2% of the nitrate in $PM_{2.5}$ in winter and 30.7 ± 11.4%, 28.3 ± 15.7%, 26.5 ± 14.4%, and 14.4 ± 6.9% in spring, respectively. The fractional contributions of coal combustion gradually increased in winter. These results are useful for reducing NO_x emissions in urban environments and clarifying the relationship between regional NO_x emissions and atmospheric NO_3^- pollution or deposition.

* Corresponding author.
E-mail address: guanhui@mail.gyig.ac.cn (H. Guan).

https://doi.org/10.1016/j.atmosenv.2022.119036
Received 19 December 2021; Received in revised form 2 March 2022; Accepted 2 March 2022
Available online 5 March 2022

1. Introduction

Particulate pollution is receiving increasing attention in China due to due to serious pollution events. (Thishan Dharshana et al., 2010; Venecek et al., 2019). Such pollution episodes are one of the greatest environmental issues in China. Fine particles ($PM_{2.5}$) is the primary cause of haze pollution, which can be directly emitted (primary) or formed through multiphase gas-to particle conversion processes (secondary) in the atmosphere. Sulfates and nitrates from aqueous generation are considered to be major sources of secondary formation in $PM_{2.5}$ (Quan et al., 2014; Dong et al., 2020). Nitrate is a major part of atmospheric aerosols. However, nitrate aerosols affect the surface temperature of the Earth, acid rain formation, and human health (Wang and Wang, 2014), playing a key role in environmental chemistry and climate change (Twomey, 1977; Albrecht, 1989). Therefore, determining the source(s) of aerosol nitrate and its transport and transformation in the atmosphere will provide the necessary basis for improving air quality.

Nitrogen oxides ($NO_x = NO + NO_2$) are the precursors of atmospheric nitric acid (Fang et al., 2011). Anthropogenic nitrogen oxides are emitted during fossil fuel combustion and from vehicles (Galloway et al., 2004), whereas lightning, biomass burning, and biological soil emissions are natural sources of NO_x (Galanter et al., 2000; Schumann and Huntrieser, 2007; Hudman et al., 2012), and there is uncertainty over their relative contributions. The sources of atmospheric NO_x were studied by field measurements of NO_x emissions from particular point sources (such as coal-fired power plants (Ma et al., 2016) and gas-fired boilers (Yue et al., 2018). However, such observations are difficult to use in regional NO_x inventories. The Comprehensive Air Quality Model (CAMx) and Community Multiscale Air Quality (CMAQ) are usually accompanied by some level of uncertainty that may lead to differences in the magnitude of source contributions (Han et al., 2009; Zhao et al., 2013). Although satellite data coupled with models can both evaluate large-scale NO_x fluxes and distinguish NO_x sources (Lu et al., 2016; Ding et al., 2017), the results of the model rely on in-situ observations. Since NO_x is mainly oxidized to granular nitrate in heavily polluted areas, $\delta^{15}N$ is considered to be an effective tool for identifying the source of aerosol NO_3^-. Although the impact of kinetic and equilibrium isotopic fractionation of $\delta^{15}N$ during the conversion of NO_x to NO_3^- and the isotopic effect of $\delta^{15}N$-$\delta^{18}O$ associated with NO_x oxidation must be considered (Walters et al., 2016). Previous studies of $\delta^{15}N$– NO_3^- have largely produced qualitative descriptions of possible sources (Hastings et al., 2003; Elliott et al., 2009; Altieri et al., 2013). However, that isotopic techniques can only reveal source information qualitatively, and that methods for providing accurate quantitative estimates need to be further explored. In recent studies improved the Bayesian model for apportioning atmospheric NO_x sources and quantitatively apportioned the respective contribution of major sources for NO_x in southwest China (Liu et al., 2017); Bohai Sea (Zong et al., 2017) and Beijing (Luo et al., 2019).

The oxidation pathways, leading to the formation of atmospheric NO_3^-, have been evaluated using $\delta^{18}O$ of NO_3^-, because different oxidants participate in NO_x cycle and NO_3^- formation, and their nitrogen isotope values are also different. There are multiple pathways of NO_3^- formation. The N_2O_5 and OH pathways are the most important pathways, and are influenced by several factors such as temperature, humidity, and aerosol surface reactivity (Wankel et al., 2010). In Asia, $\delta^{18}O$–O_3 values are generally between 90‰ and 122‰, while $\delta^{18}O$–OH concentrations are generally between −15‰ and 0‰ (Johnston and Thiemens, 1997; Fang et al., 2011). Throughout its creation in the environment, the mass-independent fractionation of ozone brings about unique isotopic singularities of ozone molecules. The information of oxidants involved in the $\delta^{18}O$–NO_3^- value was used to analyse the conversion of nitrogen oxides to nitrate (Hastings et al., 2003; Hastings et al., 2004; Savarino et al., 2007; Morin et al., 2009, Tsunogai et al., 2010; Xiao et al., 2015; Bourgeois et al., 2018). Thus, nitrogen and oxygen isotopes can also be used to investigate the oxidation processes of NO_x and nitrate transport through the atmosphere (Morin et al., 2009; Wankel et al., 2010; Kawashima and Kurahashi, 2011).

To our knowledge, the focus of current studies is mainly placed on concentration changes or the variety of a single species of $PM_{2.5}$ during a specified period, and the complete chemical composition in Lanzhou is considered including sources of the particulate matter (Tan et al., 2017; Filonchyk et al., 2018; Du et al., 2020). More importantly, there is a lack of research on the isotopic composition of nitrogen compounds in the atmosphere, especially in Lanzhou. Therefore, the present research aims to determine the source of nitrogen oxides in aerosol samples collected from the urban area in Lanzhou and define the formation pathways of nitrate aerosols based on the precursor NO_x species and their variations in different seasons.

2. Methods

2.1. Sampling site and sampling details

Lanzhou is the administrative centre and biggest city of Gansu Province, located in northwest China. It is located on both sides of the Yellow River and in a valley where the Qinghai–Tibet Plateau, Inner Mongolia Plateau, and Loess Plateau intersect. It is surrounded on three sides by mountains with peaks between 1500 m and 2000 m above sea level. These topographic characteristics cause continental semi-arid climate, characterised by a low air humidity, low wind speed and frequent inversion layers in winter. The annual precipitation is 327 mm and annual mean temperature is 10.3 °C. (solar hours: 2446 h). Petrochemicals, oil refining, and manufacturing are the main industries in Lanzhou, and coal is its main energy source. Pollution events frequently occur in Lanzhou in winter (Chu et al., 2008; Li et al., 2017; Du et al., 2020). In spring, Lanzhou is affected by large sandstorms from the Gobi Desert and Tarim Basin, causing strong particulate pollution (Filonchyk et al. 2016, 2018; Wang et al., 2016).

A total of 139 aerosol samples were collected from December 1, 2017, to April 22, 2018(Winter was from December 2017 to February 2018, and Spring was from March to April 2018), at Lanzhou University (36.05°N, 103.86°E). Lanzhou University Chengguan Campus is located in the central area of Lanzhou city, which is mainly influenced by urban residents without local pollution Lanzhou is windy and still. The wind direction is easterly in spring and north-easterly in winter. The wind speed in Lanzhou is small, and the wind frequency is the most quietly wind. Samples were collected at a special high flow rate ($1.05 \pm 0.3\ m^3$/min) using quartz filters (8 × 10 in., Tissuquartz™filters, 2500 qAT-up, Pallflex, Washington, USA) and A KC-1000 sampler (Laoshan Electronic Equipment Research Institute, Qingdao, China). The sampling time started at 18:00 and lasted for 23.5 h for each sample. All samples were stored at −20 °C before chemical analysis.

The mass concentrations of $PM_{2.5}$, SO_2, NO_2, and O_3 were recorded at the China National Environmental Monitoring Centre (http://www.cnemc.cn/). Ground-based meteorological parameters (including the surface wind speed (WS), temperature (T), and RH) and meteorological observation data were sourced from the National Meteorological Center of China Meteorological Administration (http://data.cma.cn/).

2.2. Chemical and isotopic analysis

According to the method reported by (Tian et al., 2021), samples were stored at −20 °C before the experiment. In the laboratory, all sample filters before and after sampling were weighed. One-eighth filters were cut up, placed in 50 mL deionised water (Millipore, 18.2 MΩ) and subjected to ultrasound at room temperature for 30 min. The samples were centrifuged in 4200 r/min for 10 min and then the components of the supernatant were passed through a 0.22 μm pinhole filter using a syringe, decanted into a fresh 50 mL tube, and stored in a refrigerator at −20 °C before chemical analysis and determination of dual isotopic compositions. The significant water-soluble inorganic

species in the extract were analysed utilising an ion chromatograph (model ICS-1100 and ICS-900 for anions and cations, respectively) equipped with a conductivity detector (ASRSULTRA), suppressor (ASRS-300 for the ICS-1100 and CSRS-300 for the ICS-900), separator columns (AS11-HC for anions and CS12A for cations), and guard columns (AG11-HC for anions and CG12A for cations). The precision of the analyses for every ionic species might have been superior to 5%.

The $\delta^{15}N$ and $\delta^{18}O$ values of NO_3^- were determined by the denitrification method (Yeatman et al., 2001; Casciotti et al., 2002), which is widely used for aerosols, rainwater, and snow (Savarino et al., 2007; Morin et al., 2009; Vicars et al., 2013; Felix et al., 2015; Luo et al., 2018). Samples were analysed to determine the dual isotopic composition as previously reported by (Luo et al., 2018). In short, NO_3^- was reduced to N_2O by *Pseudomonas aureofaciens* (ATCC 13985) without N_2O reductase. Then GasBench-II and continuous flow isotope ratio mass spectrometer (IRMS; Thermo Fisher DELTA V advantage; Thermo Fisher Scientific, Inc., USA) were used for on-line analysis of dual isotopes of N_2O. Four international standards (USGS32, USGS34, USGS35, and IAEA-N3) and a laboratory standard were used to correct for the variations observed in the measured data. The standard deviations of the replicate measurements of these standards were better than ±0.2‰ for $\delta^{15}N$, and ±0.5‰ for $\delta^{18}O$.

2.3. Modelling analysis

2.3.1. Backward trajectories

The hybrid single-particle Lagrangian Integrated Trajectories (HYSPLIT) model and Global Data Assimilation System (GDAS) information were used to ascertain the backward trajectory every 6 h and 72 h at 500 m to analyse the origins of air masses transporting aerosols. The flight trajectories of air masses at an altitude of 500 m were calculated. The HYSPLIT model is available at the National Oceanic and Atmospheric Administration (NOAA) Air Resource Laboratory website (http://www.arl.no aa.gov/H YSPLIT.php).

2.3.2. Bayesian isotopic mixing model

The Bayesian isotopic mixing model can estimate the contribution of each source to a mixture, and the uncertainties associated with multiple sources are explicitly considered in the simulation, which the uncertainties were evaluated for the $\delta^{15}N$ variabilities of major nitrogen sources (using the $\delta^{15}N$ values of each source, expressed as mean ± SD, as inputs). At the same time, isotope fractionation during the formation of different mixture components is also taken into account (Parnell et al., 2013).

The mixing model (Parnell et al., 2010) can be expressed by defining a set of N-mixture measurements for J isotope by k source contributors, as follows:

$$Xij = \sum_{k=1}^{k} F_k \cdot (Sjk + Cjk) + ?jk \quad (1)$$

$S_{jk} \sim N(\mu_{jk}; \omega_{jk}^2)$

$C_{jk} \sim N(\lambda jk; \tau jk^2)$

$\varepsilon_{jk} \sim N(0; \sigma_j^2)$

Where all F values sum to unity; X_{ij} is the isotope value j of the mixture i; S_{jk} is the source value k for isotope j (k = 1, 2, 3, …, K), and is normally distributed with a mean μ_{jk} and standard deviation ω_{jk}. F_k is the proportion of source k estimated by the SIAR model; c_{jk} is the fractionation factor for isotope j on source k and is normally distributed with a mean λ_{jk} and standard deviation τ_{jk}. ε_{jk} is the residual error representing the additional unquantified variation between individual mixtures, and is normally distributed with a mean of 0 and a standard deviation σ_j, as described in detail elsewhere (Moore and Semmens, 2008; Jackson et al., 2009; Parnell et al., 2010).

In this section, we attempted to use $\delta^{15}N$– NO_3^- combined with SIAR model to quantify the potential sources of particulate nitrate in Lanzhou during the sampling period. According to previous studies, fractionation values obtained in controlled studies were very high, according to which the $\delta^{15}N$– NO_3^- values in particulates would be at least 52‰ higher than that of NO_x. Accordingly, the isotope fractionations during the NO_x oxidation processes, we considered that the available fractionation values might not be directly applicable to source analysis of this study. To further interpret the observed $\delta^{15}N$ – NO_3^- values in $PM_{2.5}$ for relative contributions of major NO_x sources, we calculated the ε values using the method of (Walters and Michalski, 2015; Walters et al., 2016; Zong et al., 2017).

Atmospheric NO_2 is first converted to the HNO_3 through two dominant reactions (i.e., reactions of NO_2 with OH· and N_2O_5 with H_2O) and the HNO_3 is then converted to NO_3^- (p). So far, the isotope effect between HNO_3 and NO_3^- is negligible (Walters et al., 2016; Zong et al., 2017; Chang et al., 2018), i.e., the $\delta^{15}N$–HNO_3 equals the $\delta^{15}N$– NO_3^-. Therefore, the overall isotope effects (i.e., the ε values in our study) of atmospheric NO_2 conversion to NO_3^- (p) were determined by the contributions of the above two reactions (f_{OH} and f_{N2O5}, respectively) to the oxidations of NO_2 to HNO_3 formation.

$$\varepsilon = f_{OH} \times \varepsilon_{OH} + f_{N2O5} \times \varepsilon_{N2O5} \text{ (Eqn 1)}$$

In which $f_{OH} + f_{N2O5} = 1$, ε_{OH} and ε_{N2O5} values are isotope fractionations during the above two reactions, respectively.

Because both reactions of NO_2 with OH· and N_2O_5 with H_2O are exchange reactions, both ε_{OH} and ε_{N2O5} values reflect isotope equilibrium effects in respective reaction. The ε_{OH} values can be calculated using the following mass-balance equation (Walters et al., 2016).

$$\varepsilon_{OH} = 1000 \times ((^{15}\alpha_{NO2/NO} - 1)(1 - f_{NO2}) / ((1 - f_{NO2}) + (^{15}\alpha_{NO2/NO} \times f_{NO2})) \text{ (Eqn 2)}$$

Where the $^{15}\alpha_{NO2/NO}$ value is the equilibrium isotope fractionation factor between NO_2 and NO, which is a temperature-dependent function (see Eqn (4)), and the f_{NO2} is the fraction of NO_2 in the total NO_x. The f_{NO2} values is from 0.2 to 0.95. Similarly, the ε_{N2O5} values can be calculated from the following equation (Walters et al., 2016)

$$\varepsilon_{N2O5} = 1000 \times (^{15}\alpha_{N2O5/NO2} - 1) \quad \text{(Eqn 3)}$$

In which the $^{15}\alpha_{N2O5/NO2}$ refers to the equilibrium isotope effects between N_2O_5 and NO_2, which is a temperature-dependent function (see Eqn (4)). The $^{15}\alpha_{NO2/NO}$ and $^{15}\alpha_{N2O5/NO2}$ in Eqns (2) and (3) (expressed the $^{15}\alpha_{X/Y}$) were calculated by Eqn (4):

$$1000\,(^{15}\alpha_{X/Y}\text{-}1) = A / T^4 \times 10^{10} + B / T^3 \times 10^8 + C / T^2 \times 10^6 + D / T \times 10^4 \text{ (Eqn 4)}$$

Where A = 3.8834, B = −7.7299, C = 6.0101 and D = −0.17928 for $^{15}\alpha_{NO2/NO}$; and A = 0.69398, B = −1.9859, C = 2.3876 and D = −0.16308 for $^{15}\alpha_{N2O5/NO2}$ (Walters and Michalski, 2015). In the study, the temperature (T) is shown in Fig. 1a.

The f_{OH} and f_{N2O5} values were determined by the ^{18}O fractionations of the above two reactions, respectively e (Walters et al., 2016; Zong et al., 2017; Chang et al., 2018), which can be expressed in Eqn (5).

$$\delta^{18}O\text{–}NO_3^- = [\delta^{18}O\text{–}NO_3^-]_{OH} \times f_{OH} + [\delta^{18}O\text{–}NO_3^-]_{N2O5} \times f_{N2O5} \text{ (Eqn 5)}$$

Where $f_{OH} + f_{N2O5} = 1$. The $[\delta^{18}O\text{–}NO_3^-]_{OH}$ was calculated by the following equations (Eqn (6)).

$$[\delta^{18}O\text{–}NO_3^-]_{OH} = 2/3 \times [\delta^{18}O\text{–}NO_2]_{OH} + 1/3 \times [\delta^{18}O\text{–}OH]_{OH} \text{ (Eqn 6)}$$

Where the $[\delta^{18}O\text{–}NO_2]_{OH}$ and $[\delta^{18}O\text{–}OH]_{OH}$ values were calculated by Eqn (7) and Eqn (8), respectively.

$$[\delta^{18}O\text{–}NO_2]_{OH} = 1000 \times (^{18}\alpha_{NO2/NO} - 1) \times (1\text{-}f_{NO2})/((1\text{-}f_{NO2}) + (^{18}\alpha_{NO2/NO} \times f_{NO2})) + [\delta^{18}O\text{-}NO_x] \text{ (Eqn 7)}$$

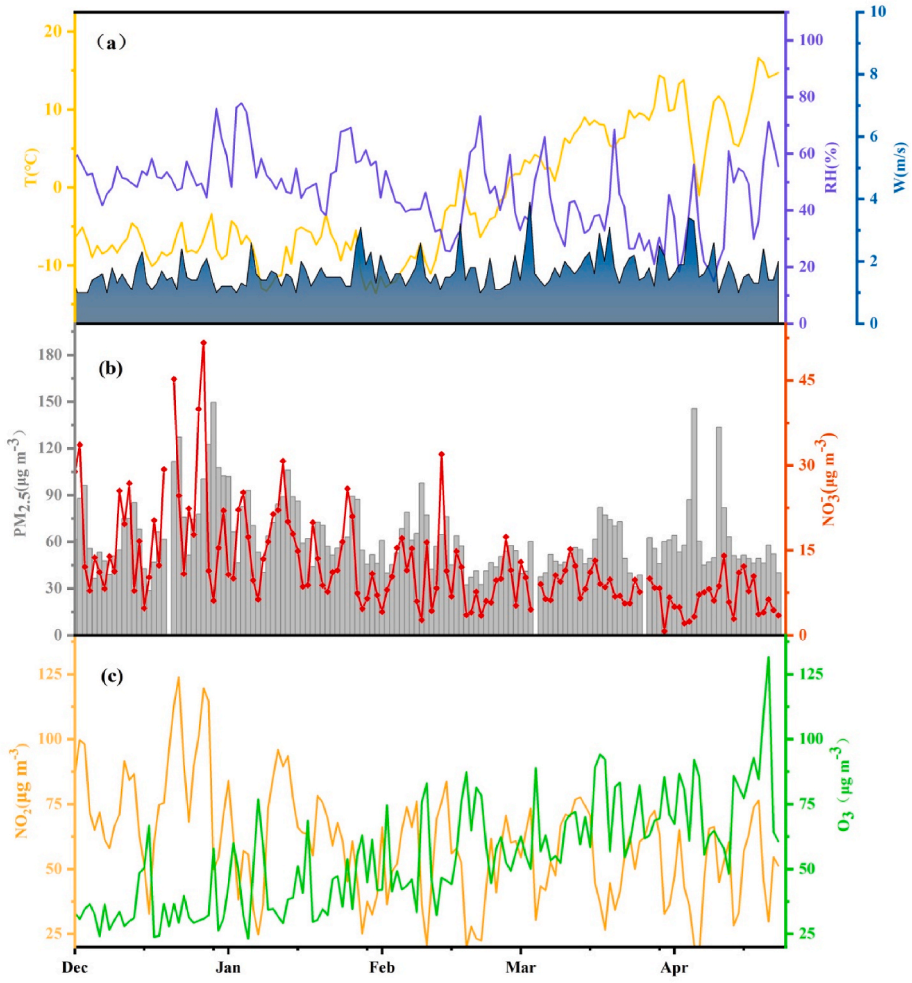

Fig. 1. Temporal variations of T, RH and W (a), $PM_{2.5}$, NO_3^- (b) concentrations, and NO_2, O_3, (c) concentrations from Dec 2017 to Apr 2018.

$$[\delta^{18}O\text{–}OH]_{OH} = (\delta^{18}O\text{–}H_2O) + 1000 \times ({}^{18}\alpha_{OH/H2O} - 1) \quad \text{(Eqn 8)}$$

In Eqn (7) and Eqn (8), the ${}^{18}\alpha_{NO/NO2}$ and ${}^{18}\alpha_{OH/H2O}$ (expressed as the ${}^{18}\alpha_{X/Y}$) values were calculated by the following equation (Eqn (9)).

$$1000({}^{18}\alpha_{X/Y}\text{-}1) = A / T^4 \times 10^{10} + B / T^3 \times 10^8 + C / T^2 \times 10^6 + D / T \times 10^4 \quad \text{(Eqn 9)}$$

Where A = −0.04129, B = 1.1605, C = −1.8829 and D = 0.74723 for ${}^{18}\alpha_{NO/NO2}$; and A = 2.1137, B = −3.8026, C = 2.2653 and D = 0.5941 for ${}^{18}\alpha_{H2O/OH}$ (Walters et al., 2016). In our study, the temperature (T) data is shown in Fig. 1a.

The $[\delta^{18}O\text{–}NO_3^-]_{N2O5}$ values in Eqn (5) were calculated by Eqn (10).

$$[\delta^{18}O\text{–}NO_3^-]_{N2O5} = 5/6 \times (\delta^{18}O\text{–}N_2O_5) + 1/6 \times (\delta^{18}O\text{–}H_2O) \quad \text{(Eqn 10)}$$

In Eqn (10), the $\delta^{18}O\text{–}H_2O$ values were estimated as the $\delta^{18}O$ values of tropospheric water vapor (−12.5 ± 17.6‰) (Walters et al., 2016), and the $\delta^{18}O\text{–}N_2O_5$ values were (126.4 ± 7.1)‰ (Walters et al., 2016).

The NO_3^- of $PM_{2.5}$ in Lanzhou, a Monte Carlo simulation was performed to generate 10000 feasible solutions, which determined that the error between predicted and measured $\delta^{18}O$ was less than 0.5‰. The standard deviations of each variable in the above calculations were estimated by the Monte Carlo method and were finally propagated into the uncertainties of the $\varepsilon_{(NO2\rightarrow HNO3)}$ values. These $\varepsilon_{(NO2\rightarrow HNO3)}$ values were considered the $\delta^{18}O\text{–}NO_3^-$ based calculation (Zong et al., 2017). found that the model results with 0.52 times the equilibrium fractionation value had the highest probability distribution of all source contributions and were considered to be the final solution in this study.

3. Results and discussion

3.1. Chemical characteristics of $PM_{2.5}$

The $PM_{2.5}$ concentration ranged from 28.7 μg m^{-3} to 149.5 μg m^{-3}, with an average of 63.1 ± 22.6 μg m^{-3}; this value is fundamentally higher than that recommended by the world Health Organization (35 μg m^{-3}). The results of the variation of $PM_{2.5}$ mass concentration are presented in Table 1 and Fig. 1b; the concentration was 28.7 μg m^{-3}–149.5 μg m^{-3} during the winter (mean of 66.3 ± 23.1 μg m^{-3}), that is, higher than that in spring (31.2 μg m^{-3}–145.5 μg m^{-3}, mean of 57.5 ± 27.6 μg m^{-3}). These results can be attributed to the increase in coal burning for domestic heating and the enhancement in the stability of the atmospheric boundary layer during winter (Cao et al., 2005; Xiao et al., 2014).

Water-soluble inorganic ions (WSIIs) were the major components of $PM_{2.5}$ in Lanzhou (Table 1). The NO_3^-, SO_4^{2-}, and NH_4^+ concentrations and atmospheric conditions (e.g., T, RH, and gas precursors) exhibited seasonal changes (Fig. 1; Table 1). The NO_3^- and NH_4^+ concentrations were relatively high in winter than in spring. The higher NO_3^- and NH_4^+ contents observed in our study could be ascribed to the transformation of NH_3 (g) into NH_4^+ (p) and that of HNO_3 (g) into NO_3^- (p) at low ambient temperature conditions. Table 1 show that the SO_4^{2-} concentration was slightly lower in winter than in spring, and the SO_2 concentration decreased in spring. WS and SO_4^{2-} concentrations were

Table 1
Mean (and standard deviation) seasonal concentrations of $PM_{2.5}$ mass, ionic species, and gaseous pollutants along with the mean ambient temperature and mean relative humidity measured in Lanzhou from Dec 2017 to Apr 2018.

Component (unit)	Winter		Spring		Annual value	
	Mean	Range	Mean	Range	Mean	Range
$PM_{2.5}$(μg m^{-3})	66.3 ± 23.1	28.7–149.5	57.5 ± 20.6	31.2–145.5	63.1 ± 22.6	28.7–149.5
Cl^-(μg m^{-3})	3.1 ± 1.9	0.5–12.7	2.7 ± 2.1	0.3–11.1	2.9 ± 2.0	0.3–12.7
NO_3^-(μg m^{-3})	14.7 ± 9.3	2.7–51.6	7.7 ± 3.2	0.7–15.2	12.2 ± 8.4	0.7–51.6
SO_4^{2-}(μg m^{-3})	14.3 ± 6.7	5.6–49.2	11.9 ± 6.1	1.2–33.9	13.4 ± 6.6	1.2–49.2
K^+(μg m^{-3})	0.6 ± 0.4	0.1–2.8	0.7 ± 0.4	0.1–2.5	0.6 ± 0.4	0.1–2.8
Na^+(μg m^{-3})	1.4 ± 1.8	0.1–12.9	2.1 ± 2.0	0.2–9.2	1.7 ± 1.9	0.1–12.9
Ca^{2+}(μg m^{-3})	4.3 ± 5.1	1.4–17.4	9.7 ± 3.8	3.1–23.5	6.8 ± 3.6	1.4–23.5
Mg^{2+}(μg m^{-3})	0.2 ± 0.2	0.1–1.4	0.6 ± 0.4	0.1–2.4	0.4 ± 0.3	0.1–2.4
NH_4^+(μg m^{-3})	7.6 ± 4.2	1.3–24.9	3.6 ± 1.6	0.1–6.6	6.2 ± 4.0	0.1–24.9
NO_2 (μg m^{-3})	64.3 ± 23.0	19.3–123.9	52.6 ± 15.9	16.8–77.6	60.0 ± 21.4	16.8–123.9
SO_2 (μg m^{-3})	39.7 ± 14.5	10.6–71.0	19.5 ± 8.3	5.3–42.8	32.2 ± 15.9	4.5–71.0
O_3(μg m^{-3})	44.5 ± 15.6	23.1–87.4	72.1 ± 16.2	48.1–131.7	54.7 ± 20.7	23.1–131.7
NOR	0.14 ± 0.06	0.0–0.4	0.10 ± 0.05	0.0–0.2	0.13 ± 0.1	0.0–0.4
SOR	0.20 ± 0.09	0.1–0.5	0.30 ± 0.12	0.1–0.6	0.2 ± 0.1	0.07–0.64
$\delta^{15}N$– NO_3^-(‰)	12.0 ± 3.1	4.2–17.4	7.0 ± 3.5	0.2–16.7	10.2 ± 4.0	0.2–17.4
$\delta^{18}O$– NO_3^-(‰)	81.8 ± 6.2	66.1–96.4	73.2 ± 8.4	55.5–108.2	78.7 ± 8.2	55.5–108.2

positively correlated (r = 0.23) in spring and negatively correlated (r = −0.08) in winter, suggesting that the SO_4^{2-} concentrations are affected by external sources such as dust.

The high NO_3^-, SO_4^{2-}, and NH_4^+ concentrations indicate that many secondary pollutants are produced. The nitrogen and sulfur oxidation ratios (NOR and SOR) were used to evaluate the extent of the photochemical oxidation of NO_2 and SO_2 (Ohta and Okita, 1990; Fu et al., 2008; Luo et al., 2019). The NOR and SOR values greater than 0.1 indicate the generation of secondary nitrate and sulfate pollutants. The NOR and SOR values obtained in this study were greater than 0.1 in both seasons. Fig. 1c and Table 1 show that the NOR in winter was higher than that in spring, indicating that the photochemical oxidation reaction of NO_2 was more significant in winter. Therefore, it can be concluded that the oxidation efficiency of gaseous NO_2 is improved at low temperatures, leading to the sudden increase of NO_3^- concentration in winter (Lin and Cheng, 2007). However, the SOR is higher in spring than in winter, and the correlation between SO_4^{2-} and SO_2 is low (r = 0.06). When mineral cation concentrations are high, large amounts of SO_4^{2-} are associated with cations such as Ca^{2+}. The large increase in the mass concentration of SO_4^{2-} in spring is related to the local sand and dust weather (Wang et al., 2016). In addition, the aerosol Cl^- mainly originates from sea salt (Luo et al., 2016) or coal combustion (Wei Xie et al., 1999; Xu et al., 2016). During the study period, it can be seen from the backward trajectories that almost all air masses come from land rather than sea (Fig. 2), which means that sea salt Cl^- was negligible in the study area. Meanwhile, we find that a positive correlation was found between the NO_3^- values and Cl^- concentrations of $PM_{2.5}$ (r = 0.43, p < 0.01) in winter, further indicates that Cl^- mainly originates from coal combustion in city environments.

3.2. Dual isotopes of nitrate in $PM_{2.5}$

Table 1 shows that the range of $\delta^{15}N$– NO_3^- was rather large 0.2‰–17.4‰, (mean of 10.2 ± 4.0‰). The $\delta^{18}O$– NO_3^- value ranged from 55.5‰ to 108.2‰ (mean of 78.7 ± 8.2‰) and was higher than that observed in other studies in Summit, the Gulf of Aqaba, Mt. Lulin and other cities (Table 2).

The $\delta^{15}N$ value was low in spring and high in winter; these observations were similar to those reported for northern China (Zong et al., 2017). The $\delta^{15}N$–NO_3^- values in winter (4.2‰–17.4‰, mean of 12.0 ± 3.1‰) were significantly different from those in spring (0.17‰–16.7‰, mean of 7.0 ± 3.5‰), suggesting that NO_x sources change in winter. For example, the $\delta^{15}N$ value NO_x from coal combustion is high (Felix et al., 2012), whereas those related to mobile sources or microbial processes tend to be more negative (Li and Wang, 2008; Felix and Elliott, 2014; Walters et al., 2015). Many studies have shown that NO_x sources can be traced by using the $\delta^{15}N$– NO_3^- value (Kojima et al., 2011; Altieri et al., 2013; Savarinoa et al., 2013; Geng et al., 2014). The relatively higher

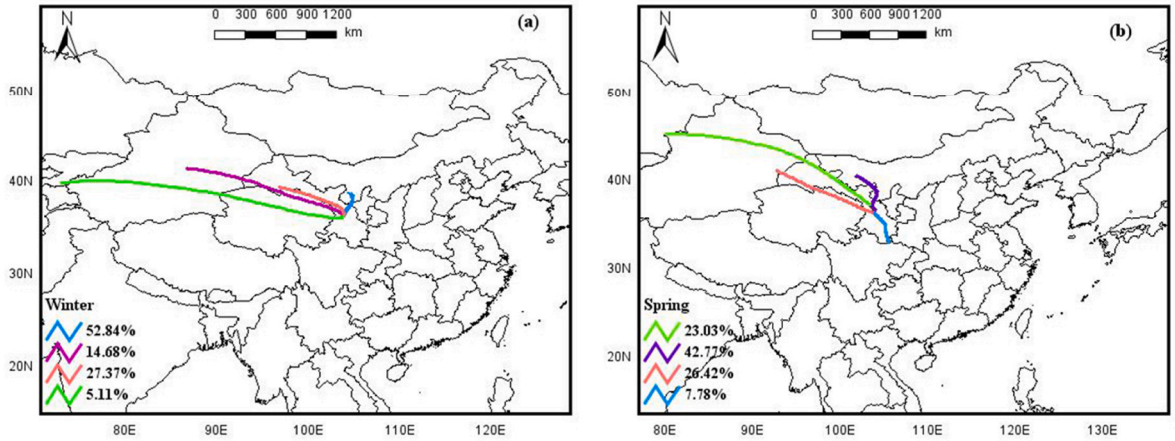

Fig. 2. Back-trajectory clustering results for 2017.12–2018.4 at Lanzhou. (a), (b) represent Winter and Spring (different color showed the trajectories and the proportion of air masses expressed as a percentage). (For interpretation of the references to color in this figure legend, the reader is referred to the Web version of this article.)

Table 2
Comparison of $\delta^{15}N–NO_3^-$ and $\delta^{18}O–NO_3^-$ data from studies in various locations worldwide.

Location	Information	Sample types	$\delta^{15}N–NO_3^-$ (‰)	$\delta^{18}O–NO_3^-$ (‰)	Reference
Summit	2001.03, 2001.08	snow	−15.3–16.7	65.~79.6	Hastings et al. (2004)
Dumont d'Urville	2001.1.16–2001.12.22	HVAS	−46.9–10.8	60–110	Savarino et al. (2007)
the coast of California	2010.5.14–2010.6.7	HVAS	−6.2–8	50.7–80.3	Vicars et al. (2013)
the Gulf of Aqaba	2003.08–2004.11	TSP	−6.9–1.9	66.1–85.3	Wankel et al. (2010)
Mt. Lulin	2010.1.13–2010.12.31	TSP	−17.2–6.5	10.8–92.4	Guha et al. (2017)
Sanjiang	2013.10.08–2013.10.18	$PM_{2.5}$	9.5–13.8	57.2–75.1	Chang et al. (2018)
Zhanjiang	2015.05–2017.11	Precipitation	−1.8–4.1	42.7–61.6	Chen et al. (2019)
Nanchang	2017.09–2017.12	$PM_{2.5}$	−10.5–12.5	34.5–91.9	Xiao et al. (2020)

$\delta^{15}N$ value may be attributed to the increase in coal combustion during winter.

In our study, the $\delta^{18}O–NO_3^-$ obtained in winter (66.1‰–96.4‰, mean of 81.8 ± 6.2‰) was higher than that in spring (56.7‰–92.5‰, mean of 75.7 ± 7.2‰). Generally, the $\delta^{18}O$ values of OH radicals range from −15‰ to 0‰ (Fang et al., 2011), and those of O_3 vary from 90‰ to 122‰ (Krankowsky et al., 1995; Johnston and Thiemens, 1997). The linear correlation between $\delta^{18}O$ and $\delta^{15}N$ is shown in Fig. 3; the correlation coefficient (r) was determined to be 0.60 ($p < 0.001$). We observed low and high NO_3^-, $\delta^{15}N$, and $\delta^{18}O$ concentrations in warmer and cooler months, respectively, which indicates that the contributions of each nitrate source and oxidation pathway changed with the change in temperature in different seasons. As previously reported, this indicates that in seasons with cooler temperatures and longer nights, O_3 plays a more important role in the formation of nitrate than OH radical with lower concentration (Elliott et al., 2009; Xiao et al. 2015, 2020). In spring, the $\delta^{18}O$ values were higher in Lanzhou than those reported from other regions worldwide (Table 2). The aerosol samples might contain high concentrations of mineral dust, which has a highly reactive surface (Hanisch and Crowley, 2001; Mogili et al., 2006; Wankel et al., 2010). The mineral dust particles in tropospheric aerosols provide surfaces for the adsorption and reaction of trace atmospheric gases (Usher et al., 2003). The results of previous studies have shown that heterogeneous reactions of N_2O_5 with mineral dust aerosols lead to the reduction of the NO_x and O_3 concentrations and the aerosol components of the mineral dust have a catalytic effect on the reactions. Thus, O_3 and mineral dust plays a greater role in spring in Lanzhou.

3.3. Source apportionment of $\delta^{15}N–NO_3^-$ in $PM_{2.5}$

In this study, the uncertainty of ε ($NO_2 \rightarrow HNO_3$) values was obtained by Monte Carlo method, and these ε ($NO_2 \rightarrow HNO_3$) values were calculated from $\delta^{18}O–NO_3^-$ measurements. The ε value was calculated to be 9.7 ± 0.41‰ in winter and 8.8 ± 0.42‰ in spring. The main contributors of the NO_x in this study were coal combustion (13.7 ± 4.6‰) (Felix et al. 2012, 2015; Walters and Michalski, 2015), vehicle exhausts (−7.2 ± 6.1‰) (Moore, 1977, Heaton, 1990, Ammann et al., 1999; Felix and Elliott, 2014, Walters et al., 2015), biomass burning (1.0 ± 4.1‰) (Fibiger and Hastings, 2016), and biogenic soil emissions (−30.1 ± 9.2‰) (Li and Wang, 2008; Felix and Elliott, 2014). The contribution fraction of NO_x from different sources to NO_3^- was determined by the Bayesian model calculation (Fig. 4); these sources contributed to NO_x in the following decreasing order: coal combustion > biomass burning > vehicle exhausts > soil microbial emissions, with the respective values in winter (spring) being 42.2 ± 9.9% (30.7 ± 11.4%), 27.8 ± 16.2% (28.3 ± 15.7%), 22.2 ± 12.3% (26.5 ± 14.4%), and 7.7 ± 5.2% (14.4 ± 6.9%). These data showed that the contribution of coal combustion to NO_x was higher in winter, indicating that coal combustion is the dominant source of NO_x during the cooler months in Lanzhou. The results mentioned above are consistent with the previous research results in Lanzhou (Qiu et al., 2016). Our experiments confirm that the contribution rate of NO_x sources vary in different seasons.

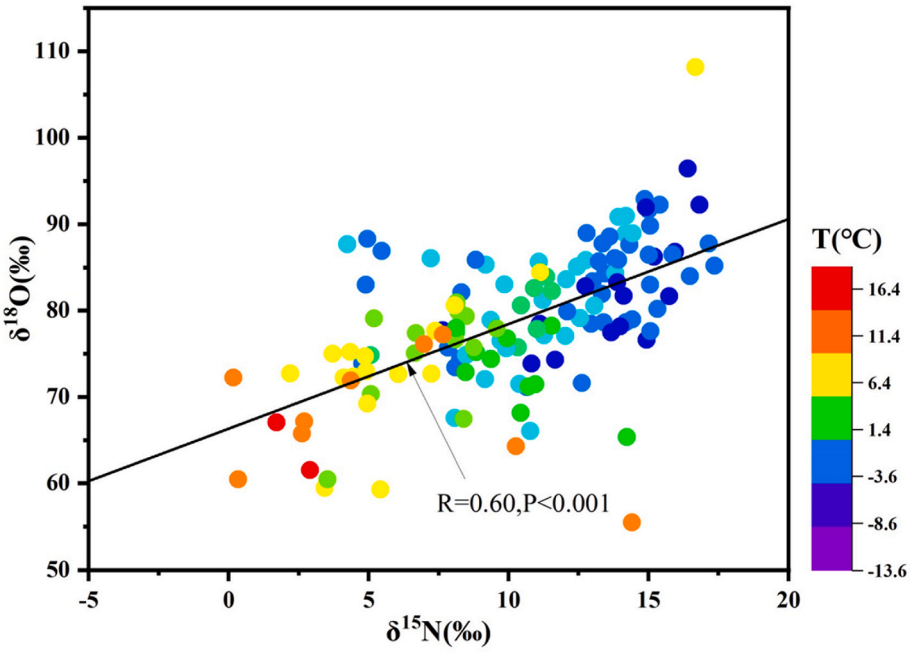

Fig. 3. The correlation plot between $\delta^{15}N$ and $\delta^{18}O$ values and color represent temperature. (For interpretation of the references to color in this figure legend, the reader is referred to the Web version of this article.)

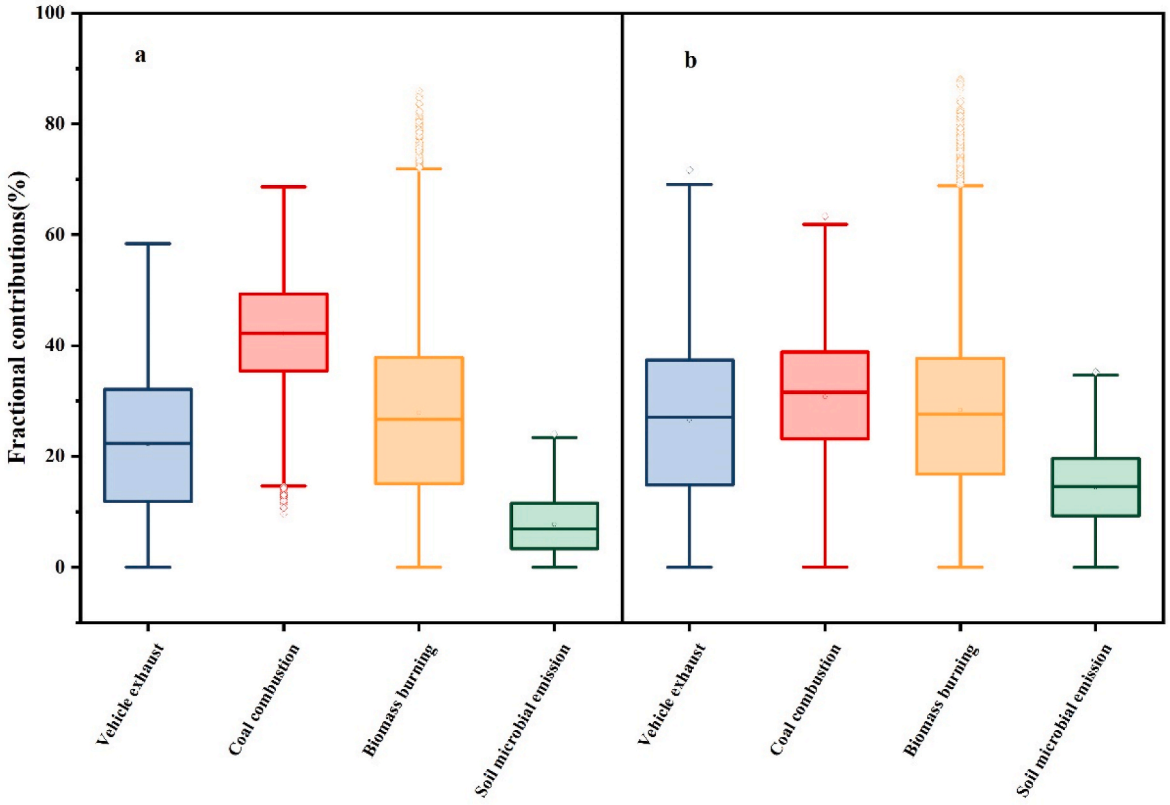

Fig. 4. Box plots of the fractional contributions of coal combustion, biomass burning, vehicle exhaust and soil emission in 2017–2018 in Lanzhou, during the (a) Winter, and (b) Spring. The box encompasses the 25th–75th percentiles, and the whiskers are the 5th and 95th percentiles. The lines inside the boxes indicate the median values and the diamonds represent to mean values.

4. Conclusion

Our results showed that the $PM_{2.5}$ concentration ranged from 28.9 μg m^{-3} to 149.5 μg m^{-3} (average 63.1 ± 22.6 μg m^{-3}), and nitrate, sulfate, calcium, and ammonium were the dominant species. The main reasons for serious pollution are weak convection and inversion layer in winter in Lanzhou, which makes it difficult for pollutants to transport and aggravates the pollution level. In addition, high humidity conditions are conducive to the formation of new particles. Secondary sand-blowing or dusty weather in spring also exacerbates pollution.

The $\delta^{15}N$ value of NO_3^- varied from 0.2‰ to 17.4‰ (mean value of 10.2 ± 4.0‰) and the $\delta^{18}O$ of the nitrate ranged from 55.5‰ to 108.2‰ (mean value of 78.7 ± 8.2‰). The $\delta^{15}N$ and $\delta^{18}O$ values showed strong seasonal variation, indicating that the sources of NO_x and the oxidation pathways of nitrate change from winter to spring in Lanzhou.

According to the Bayesian isotope mixing model, the contribution rate of NO_x sources differ in different seasons. Although coal burning is the main source in spring and winter, the contribution rate of soil microbial emissions gradually increases with the increase of temperature. The measurement of nitrogen and oxygen isotopes using isotope technology and Bayesian model simulation for the first time in Lanzhou will help clarifying the relationships between regional NO_x emissions and atmospheric NO_3^- pollution or deposition. Furthermore, these will be helpful in reducing NO_x emissions in urban environments, thereby contributing toward mitigating air pollution.

CRediT authorship contribution statement

Meiju Yin: Methodology, Data curation, Writing – original draft. **Hui Guan:** Conceptualization, Methodology, Supervision, Writing – review & editing. **Li Luo:** Methodology, Supervision, Writing – review & editing. **Huayun Xiao:** Data curation, Investigation. **Zhongyi Zhang:** Data curation, Investigation.

Declaration of competing interest

The authors declare that they have no known competing financial interests or personal relationships that could have appeared to influence the work reported in this paper.

Acknowledgments

This study was kindly supported by the National Natural Science Foundation of China through grant numbers 41425014, 41603017 and 41863001, the National Key Research and Development Program of China through grant number 2016YFA0601000.

References

Albrecht, B.A., 1989. Aerosols, cloud microphysics, and fractional cloudiness. Science 245, 1227–1230.

Altieri, K.E., Hastings, M.G., Gobel, A.R., Peters, A.J., Sigman, D.M., 2013. Isotopic composition of rainwater nitrate at Bermuda: the influence of air mass source and chemistry in the marine boundary layer. J. Geophys. Res. Atmos. 118, 11304–11316.

Ammann, M., Siegwolf, R., Pichlmayer, F., Suter, M., Saurer, M., Brunold, C., 1999. Estimating the uptake of traffic-derived NO_2 from ^{15}N abundance in Norway spruce needles. Oecologia 118, 124–131.

Bourgeois, I., Savarino, J., Caillon, N., Angot, H., Barbero, A., Delbart, F., Voisin, D., Clement, J.C., 2018. Tracing the fate of atmospheric nitrate in a subalpine watershed using delta $\triangle^{17}O$. Environ. Sci. Technol. 52, 5561–5570.

Cao, J.J., Wu, F., Chow, J.C., Lee, S.C., Li, Y., Chen, S.W., An, Z.S., Fung, K.K., Watson, J. G., Zhu, C.S., Liu, S.X., 2005. Characterization and source apportionment of atmospheric organic and elemental carbon during fall and winter of 2003 in Xi'an, China. Atmos. Chem. Phys. 5, 3127–3137.

Casciotti, K.L., Sigman, D.M., Hastings, M.G., Bohlke, J.K., Hilkert, A., 2002. Measurement of the oxygen isotopic composition of nitrate in seawater and freshwater using the denitrifier method. Anal. Chem. 74, 4905–4912.

Chang, Y., Zhang, Y., Tian, C., Zhang, S., Ma, X., Cao, F., Liu, X., Zhang, W., Kuhn, T., Lehmann, M.F., 2018. Nitrogen isotope fractionation during gas-to-particle conversion of NO_x to NO_3^- in the atmosphere – implications for isotope-based NOx source apportionment. Atmos. Chem. Phys. 18, 11647–11661.
Chen, F.J., Lao, Q.B., Jia, G.D., Chen, C.Q., Zhu, Q.M., Zhou, X., 2019. Seasonal variations of nitrate dual isotopes in wet deposition in a tropical city in China. Atmos. Environ. 196, 1–9.
Chu, P.C., Chen, Y.C., Lu, S.H., 2008. Atmospheric effects on winter SO_2 pollution in Lanzhou, China. Atmos. Res. 89, 365–373.
Ding, J., Miyazaki, K., van der A, R.J., Mijling, B., Kurokawa, J.-i., Cho, S., Janssens-Maenhout, G., Zhang, Q., Liu, F., Levelt, P.F., 2017. Intercomparison of NO_x emission inventories over east asia. Atmos. Chem. Phys. 17, 10125–10141.
Dong, Z., Su, F., Zhang, Z., Wang, S., 2020. Observation of chemical components of $PM_{2.5}$ and secondary inorganic aerosol formation during haze and sandy haze days in Zhengzhou, China. J. Environ. Sci. (China) 88, 316–325.
Du, T., Wang, M., Guan, X., Zhang, M., Zeng, H.Y., Chang, Y., Zhang, L., Tian, P.F., Shi, J. S., Tang, C.G., 2020. Characteristics and formation mechanisms of winter particulate pollution in Lanzhou, northwest China. J. Geophys. Res. Atmos. 125.
Elliott, E.M., Kendall, C., Boyer, E.W., Burns, D.A., Lear, G.G., Golden, H.E., Harlin, K., Bytnerowicz, A., Butler, T.J., Glatz, R., 2009. Dual nitrate isotopes in dry deposition: utility for partitioning NO_x source contributions to landscape nitrogen deposition. J. Geophys. Res. 114.
Fang, Y.T., Koba, K., Wang, X.M., Wen, D.Z., Li, J., Takebayashi, Y., Liu, X.Y., Yoh, M., 2011. Anthropogenic imprints on nitrogen and oxygen isotopic composition of precipitation nitrate in a nitrogen-polluted city in southern China. Atmos. Chem. Phys. 11, 1313–1325.
Felix, J.D., Elliott, E.M., 2014. Isotopic composition of passively collected nitrogen dioxide emissions: vehicle, soil and livestock source signatures. Atmos. Environ. 92, 359–366.
Felix, J.D., Elliott, E.M., Shaw, S.L., 2012. Nitrogen isotopic composition of coal-fired power plant NO_x: influence of emission controls and implications for global emission inventories. Environ. Sci. Technol. 46, 3528–3535.
Felix, J.D., Elliott, E.M., Avery, G.B., Kieber, R.J., Mead, R.N., Willey, J.D., Mullaugh, K. M., 2015. Isotopic composition of nitrate in sequential Hurricane Irene precipitation samples: implications for changing NO_x sources. Atmos. Environ. 106, 191–195.
Fibiger, D.L., Hastings, M.G., 2016. First measurements of the nitrogen isotopic composition of NO_x from biomass burning. Environ. Sci. Technol. 50, 11569–11574.
Filonchyk, M., Yan, H.W., Yang, S.W., Hurynovich, V., 2016. A study of $PM_{2.5}$ and PM_{10} concentrations in the atmosphere of large cities in Gansu Province, China, in summer period. J. Earth Syst. Sci. 125, 1175–1187.
Filonchyk, M., Yan, H.W., Li, X.J., 2018. Temporal and spatial variation of particulate matter and its correlation with other criteria of air pollutants in Lanzhou, China, in spring-summer periods. Atmos. Pollut. Res. 9, 1100–1110.
Fu, Q.Y., Zhuang, G.S., Wang, J., Xu, C., Huang, K., Li, J., Hou, B., Lu, T., Streets, D.G., 2008. Mechanism of formation of the heaviest pollution episode ever recorded in the Yangtze River Delta, China. Atmos. Environ. 42, 2023–2036.
Galanter, M., Levy, H., Carmichael, G.R., 2000. Impacts of biomass burning on tropospheric CO, NO_x, and O_3. J. Geophys. Res. Atmos. 105, 6633–6653.
Galloway, J.N., Dentener, F.J., Capone, D.G., Boyer, E.W., Howarth, R.W., Seitzinger, S. P., Asner, G.P., Cleveland, C.C., Green, P.A., Holland, E.A., Karl, D.M., Michaels, A. F., Porter, J.H., Townsend, A.R., Vorosmarty, C.J., 2004. Nitrogen cycles: past, present, and future. Biogeochemistry 70, 153–226.
Geng, L., Alexander, B., Cole-Dai, J., Steig, E.J., Savarino, J., Sofen, E.D., Schauer, A.J., 2014. Nitrogen isotopes in ice core nitrate linked to anthropogenic atmospheric acidity change. Proc. Natl. Acad. Sci. U. S. A. 111, 5808–5812.
Guha, T., Lin, C.T., Bhattacharya, S.K., Mahajan, A.S., Ou-Yang, C.F., Lan, Y.P., Hsu, S.C., Liang, M.C., 2017. Isotopic ratios of nitrate in aerosol samples from Mt. Lulin, a high-altitude station in Central Taiwan. Atmos. Environ. 154, 53–69.
Han, K.M., Song, C.H., Ahn, H.J., Park, R.S., Woo, J.H., Lee, C.K., Richter, A., Burrows, J. P., Kim, J.Y., Hong, J.H., 2009. Investigation of NOx emissions and NO_x-related chemistry in East Asia using CMAQ-predicted and GOME-derived NO_2 columns. Atmos. Chem. Phys. 9, 1017–1036.
Hanisch, F., Crowley, J.N., 2001. Heterogeneous reactivity of gaseous nitric acid on Al_2O_3, $CaCO_3$, and atmospheric dust samples: a knudsen cell study. J. Phys. Chem. 105, 3096–3106.
Hastings, M.G., Sigman, D.M., Lipschultz, F., 2003. Isotopic evidence for source changes of nitrate in rain at Bermuda. J. Geophys. Res. Atmos. 108, 4709.
Hastings, M.G., Steig, E.J., Sigman, D.M., 2004. Seasonal variations in N and O isotopes of nitrate in snow at Summit, Greenland: implications for the study of nitrate in snow and ice cores. J. Geophys. Res. Atmos. 109.
Heaton, T.H.E., 1990. 15N/14N ratios of NO_x from vehicle engines and coal-fired power stations. Tellus 42, 304–307.
Hudman, R.C., Moore, N.E., Mebust, A.K., Martin, R.V., Russell, A.R., Valin, L.C., Cohen, R.C., 2012. Steps towards a mechanistic model of global soil nitric oxide emissions: implementation and space based-constraints. Atmos. Chem. Phys. 12, 7779–7795.
Jackson, A.L., Inger, R., Bearhop, S., Parnell, A., 2009. Erroneous behaviour of MixSIR, a recently published Bayesian isotope mixing model: a discussion of Moore & Semmens (2008). Ecol. Lett. 12, E1–E5.
Johnston, J.C., Thiemens, M.H., 1997. The isotopic composition of tropospheric ozone in three environments. J. Geophys. Res. Atmos. 102, 25395–25404.
Kawashima, H., Kurahashi, T., 2011. Inorganic ion and nitrogen isotopic compositions of atmospheric aerosols at Yurihonjo, Japan: implications for nitrogen sources. Atmos. Environ. 45, 6309–6316.
Kojima, K., Murakami, M., Yoshimizu, C., Tayasu, I., Nagata, T., Furumai, H., 2011. Evaluation of surface runoff and road dust as sources of nitrogen using nitrate isotopic composition. Chemosphere 84, 1716–1722.
Krankowsky, D., Bartecki, F., Klees, G.G., Mauersberger, K., Schellenbac, K., 1995. Measurement of heavy isotope enrichment in tropospheric ozone. Geophys. Res. Lett. 22.
Li, D.J., Wang, X.M., 2008. Nitrogen isotopic signature of soil-released nitric oxide (NO) after fertilizer application. Atmos. Environ. 42, 4747–4754.
Li, H., Zhang, Q., Zhang, Q., Chen, C., Wang, L., Wei, Z., Zhou, S., Parworth, C., Zheng, B., Canonaco, F., Prévôt, A.S.H., Chen, P., Zhang, H., Wallington, T.J., He, K., 2017. Wintertime aerosol chemistry and haze evolution in an extremely polluted city of the North China Plain: significant contribution from coal and biomass combustion. Atmos. Chem. Phys. 17, 4751–4768.
Lin, Y.C., Cheng, M.T., 2007. Evaluation of formation rates of NO2 to gaseous and particulate nitrate in the urban atmosphere. Atmos. Environ. 41, 1903–1910.
Liu, X.Y., Xiao, H.W., Xiao, H.Y., Song, W., Sun, X.C., Zheng, X.D., Liu, C.Q., Koba, K., 2017. Stable isotope analyses of precipitation nitrogen sources in Guiyang, southwestern China. Environ. Pollut. 230, 486–494.
Lu, X., Yao, T., Li, Y., Fung, J.C.H., Lau, A.K.H., 2016. Source apportionment and health effect of NOx over the Pearl River Delta region in southern China. Environ. Pollut. 212, 135–146.
Luo, L., Yao, X.H., Gao, H.W., Hsu, S.C., Li, J.W., Kao, S.J., 2016. Nitrogen speciation in various types of aerosols in spring over the northwestern Pacific Ocean. Atmos. Chem. Phys. 16, 325–341.
Luo, L., Kao, S.J., Bao, H.Y., Xiao, H.Y., Xiao, H.W., Yao, X.H., Gao, H.W., Li, J.W., Lu, Y. Y., 2018. Sources of reactive nitrogen in marine aerosol over the Northwest Pacific Ocean in spring. Atmos. Chem. Phys. 18, 6207–6222.
Luo, L., Wu, Y., Xiao, H., Zhang, R., Lin, H., Zhang, X., Kao, S.J., 2019. Origins of aerosol nitrate in Beijing during late winter through spring. Sci. Total Environ. 653, 776–782.
Ma, Z., Deng, J., Li, Z., Li, Q., Zhao, P., Wang, L., Sun, Y., Zheng, H., Pan, L., Zhao, S., Jiang, J., Wang, S., Duan, L., 2016. Characteristics of NO_x emission from Chinese coal-fired power plants equipped with new technologies. Atmos. Environ. 131, 164–170.
Mogili, P.K., Kleiber, P.D., Young, M.A., Grassian, V.H., 2006. N_2O_5 hydrolysis on the components of mineral dust and sea salt aerosol: comparison study in an environmental aerosol reaction chamber. Atmos. Environ. 40, 7401–7408.
Moore, H., 1977. The isotopic composition of ammonia, nitrogen dioxide and nitrate in the atmosphere. Atmos. Environ. 11, 1239–1243.
Moore, J.W., Semmens, B.X., 2008. Incorporating uncertainty and prior information into stable isotope mixing models. Ecol. Lett. 11, 470–480.
Morin, S., Savarino, J., Frey, M.M., Domine, F., Jacobi, H.W., Kaleschke, L., Martins, J.M. F., 2009. Comprehensive isotopic composition of atmospheric nitrate in the Atlantic Ocean boundary layer from 65°S to 79°N. J. Geophys. Res. 114.
Ohta, S., Okita, T., 1990. A chemical characterization of atmospheric aerosol in sapporo. Atmos. Environ. Part a-General Topics 24, 815–822.
Parnell, A.C., Inger, R., Bearhop, S., Jackson, A.L., 2010. Source partitioning using stable isotopes: coping with too much variation. PLoS One 5, e9672.
Parnell, A.C., Phillips, D.L., Bearhop, S., Semmens, B.X., Ward, E.J., Moore, J.W., Jackson, A.L., Grey, J., Kelly, D.J., Inger, R., 2013. Bayesian stable isotope mixing models. Environmetrics 24, 387–399.
Qiu, X., Duan, L., Gao, J., Wang, S., Chai, F., Hu, J., Zhang, J., Yun, Y., 2016. Chemical composition and source apportionment of PM10 and PM2.5 in different functional areas of Lanzhou, China. J. Environ. Sci. (China) 40, 75–83.
Quan, J., Tie, X., Zhang, Q., Liu, Q., Li, X., Gao, Y., Zhao, D., 2014. Characteristics of heavy aerosol pollution during the 2012–2013 winter in Beijing, China. Atmos. Environ. 88, 83–89.
Savarino, J., Kaiser, J., Morin, S., Sigman, D.M., Thiemens, M.H., 2007. Nitrogen and oxygen isotopic constraints on the origin of atmospheric nitrate in coastal Antarctica. Atmos. Chem. Phys. 7, 1925–1945.
Savarinoa, J., Morinb, S., Erblanda, J., Granneca, F., Pateyc, M.D., Vicarsa, W., Alex, B., Achterbergc, E.P., 2013. Isotopic composition of atmospheric nitrate in a tropical marine boundary layer. Proc. Natl. Acad. Sci. Unit. States Am. 110, 17668–17673.
Schumann, U., Huntrieser, H., 2007. The global lightning-induced nitrogen oxides source. Atmos. Chem. Phys. 7, 3823–3907.
Tan, J., Zhang, L., Zhou, X., Duan, J., Li, Y., Hu, J., He, K., 2017. Chemical characteristics and source apportionment of PM2.5 in Lanzhou, China. Sci. Total Environ. 601–602, 1743–1752.
Thishan Dharshana, K.G., Kravtsov, S., Kahl, J.D.W., 2010. Relationship between synoptic weather disturbances and particulate matter air pollution over the United States. J. Geophys. Res. Atmos. 115.
Tian, J., Guan, H., Zhou, Y., Zheng, N., Xiao, H., Zhao, J., Zhang, Z., Xiao, H., 2021. Isotopic source analysis of nitrogen-containing aerosol: a study of $PM_{2.5}$ in Guiyang (SW, China). Sci. Total Environ. 760, 143935.
Tsunogai, U., Komatsu, D.D., Daita, S., Kazemi, G.A., Nakagawa, F., Noguchi, I., Zhang, J., 2010. Tracing the fate of atmospheric nitrate deposited onto a forest ecosystem in Eastern Asia using $\Delta^{17}O$. Atmos. Chem. Phys. 10, 1809–1820.
Twomey, S., 1977. The influence of pollution on the shortwave albedo of clouds. J. Atmos. Sci. 34, 1149–1152.
Usher, C.R., Michel, A.E., Grassian, V.H., 2003. Reactions on mineral dust. Chem. Rev. 103, 4883–4940.
Venecek, M.A., Yu, X., Kleeman, M.J., 2019. Predicted ultrafine particulate matter source contribution across the continental United States during summertime air pollution events. Atmos. Chem. Phys. 19, 9399–9412.
Vicars, W.C., Morin, S., Savarino, J., Wagner, N.L., Erbland, J., Vince, E., Martins, J.M.F., Lerner, B.M., Quinn, P.K., Coffman, D.J., Williams, E.J., Brown, S.S., 2013. Spatial

and diurnal variability in reactive nitrogen oxide chemistry as reflected in the isotopic composition of atmospheric nitrate: results from the CalNex 2010 field study. J. Geophys. Res. Atmos. 118, 10567–10588.

Walters, W.W., Michalski, G., 2015. Theoretical calculation of nitrogen isotope equilibrium exchange fractionation factors for various NO_y molecules. Geochem. Cosmochim. Acta 164, 284–297.

Walters, W.W., Goodwin, S.R., Michalski, G., 2015. Nitrogen stable isotope composition $\delta^{15}N$ of vehicle-emitted NOx. Environ. Sci. Technol. 49, 2278–2285.

Walters, W.W., Simonini, D.S., Michalski, G., 2016. Nitrogen isotope exchange between NO and NO_2 and its implications for $\delta^{15}N$ variations in tropospheric NO_x and atmospheric nitrate. Geophys. Res. Lett. 43, 440–448.

Wang, G., Wang, P., 2014. $PM_{2.5}$ pollution in China and its harmfulness to human health. Sci. A Technol. Rev. 32, 72–78.

Wang, Y., Jia, C., Tao, J., Zhang, L., Liang, X., Ma, J., Gao, H., Huang, T., Zhang, K., 2016. Chemical characterization and source apportionment of $PM_{2.5}$ in a semi-arid and petrochemical-industrialized city, Northwest China. Sci. Total Environ. 573, 1031–1040.

Wankel, S.D., Chen, Y., Kendall, C., Post, A.F., Paytan, A., 2010. Sources of aerosol nitrate to the Gulf of Aqaba: evidence from $\delta^{15}N$ and $\delta^{18}O$ of nitrate and trace metal chemistry. Mar. Chem. 120, 90–99.

Xiao, S., Wang, Q.Y., Cao, J.J., Huang, R.J., Chen, W.D., Han, Y.M., Xu, H.M., Liu, S.X., Zhou, Y.Q., Wang, P., Zhang, J.Q., Zhan, C.L., 2014. Long-term trends in visibility and impacts of aerosol composition on visibility impairment in Baoji, China. Atmos. Res. 149, 88–95.

Xiao, H.W., Xie, L.H., Long, A.M., Ye, F., Pan, Y.P., Li, D.N., Long, Z.H., Chen, L., Xiao, H. Y., Liu, C.Q., 2015. Use of isotopic compositions of nitrate in TSP to identify sources and chemistry in South China Sea. Atmos. Environ. 109, 70–78.

Xiao, H.W., Zhu, R.G., Pan, Y.Y., Guo, W., Zheng, N.J., Liu, Y.H., Liu, C., Zhang, Z.Y., Wu, J.F., Kang, C.A., Luo, L., Xiao, H.Y., 2020. Differentiation between nitrate aerosol formation pathways in a southeast Chinese city by dual isotope and modeling studies. J. Geophys. Res. Atmos. 125.

Xie, Wei, Pan, Wei-Ping, Riley, J.T., 1999. Behavior of chloride during coal combustion in an AFBC system. Energy Fuel. 13, 585–591.

Xu, Y., Liu, X., Zhang, P., Guo, J., Han, J., Zhou, Z., Xu, M., 2016. Role of chlorine in ultrafine particulate matter formation during the combustion of a blend of high-Cl coal and low-Cl coal. Fuel 184, 185–191.

Yeatman, S.G., Spokes, L.J., Dennis, P.F., Jickells, T.D., 2001. Comparisons of aerosol nitrogen isotopic composition at two polluted coastal sites. Atmos. Environ. 35, 1307–1320.

Yue, T., Gao, X., Gao, J., Tong, Y., Wang, K., Zuo, P., Zhang, X., Tong, L., Wang, C., Xue, Y., 2018. Emission characteristics of NO_x, CO, NH_3 and VOC_s from gas-fired industrial boilers based on field measurements in Beijing city, China. Atmos. Environ. 184, 1–8.

Zhao, B., Wang, S.X., Liu, H., Xu, J.Y., Fu, K., Klimont, Z., Hao, J.M., He, K.B., Cofala, J., Amann, M., 2013. NO_x emissions in China: historical trends and future perspectives. Atmos. Chem. Phys. 13, 9869–9897.

Zong, Z., Wang, X., Tian, C., Chen, Y., Fang, Y., Zhang, F., Li, C., Sun, J., Li, J., Zhang, G., 2017. First assessment of NO_x sources at a regional background site in north China using isotopic analysis linked with modeling. Environ. Sci. Technol. 51, 5923–5931.